Journal of Solid State Chemistry **159,** 352–361 (2001)
doi:10.1006/jssc.2001.9164, available online at http://www.idealibrary.com on IDEAL®

Synthesis, Structural Isomerism, and Magnetism of the Coordination Polymers [*M*(dca)$_2$pyz], *M* = Mn, Fe, Co, Ni and Zn, dca = Dicyanamide (N(CN)$_2^-$), and pyz = Pyrazine

Paul Jensen, Stuart R. Batten, Boujemaa Moubaraki, and Keith S. Murray[1]

School of Chemistry, Monash University, P.O. Box 23, Victoria 3800, Australia
E-mail: Keith.S.Murray@sci.monash.edu.au

Received March 20, 2001; revised March 21, 2001

IN DEDICATION TO THE LATE PROFESSOR OLIVIER KAHN FOR HIS PIONEERING CONTRIBUTIONS TO THE FIELD OF MOLECULAR MAGNETISM

The coordination polymers [*M*(dca)$_2$pyz] (*M* = Mn, Fe, Co, Ni, Zn) have been synthesized and characterized by single-crystal and powder X-ray diffraction. Two isomers have been observed. The α compounds contain two interpenetrating 3D α-Po related networks. Bidentate dca ligands bridge the metal atoms to form square-grid-like *M*(dca)$_2$ sheets, with the pyrazine ligands linking these sheets together to form the α-Po-like 3D networks. The β compounds contain interdigitated 2D sheets. The sheets consist of 1D chains of *M*(dca)$_2$ connected together by the pyrazine ligands. The α compounds display an interesting phase change that simultaneously induces twinning of the crystals. At room temperature the structures are orthorhombic *Pnma* and contain dynamic disorder of the dca ligands. However, on cooling (e.g., to 123 K) the structures become monoclinic *P*2$_1$/*n* with the dca ligands ordered, but since domains within each crystal order differently, this results in pseudo-merohedral twinning. Variable temperature and variable field magnetic studies have shown that these compounds display weak antiferromagnetic coupling between the high-spin metal centers. Only in the case of α-[Mn(dca)$_2$pyz] is there evidence for 3D antiferromagnetic order occurring below 2.7 K.

Key Words: **structure; magnetism; crystal engineering; coordination polymer; dicyanamide; pyrazine; interpenetration.**

The crystal engineering of coordination polymers containing the dicyanamide (dca, N(CN)$_2^-$) ligand has attracted great interest since the initial reports of long-range magnetic ordering in the rutile-like *M*(dca)$_2$ compounds (1–4). Modification of network topology through the use of both bridging and terminal coligands has resulted in many interesting new network topologies, and the magnetic properties of these systems have also been studied (3–7). New structures have also been achieved through use of tetrahedral metal ions (3) or increasing the dca-to-metal ratio, resulting in the incorporation of countercations, which template the anionic *M*(dca)$_3^-$ networks (8).

We are especially interested in coordination polymers of dca that contain coligands that are also bridging. In particular, we have been investigating the bridging pyridyl-donor coligands pyrazine (pyz) and 4,4′-bipyridine. We have previously reported the structures and magnetic properties of both the α and β phases of [Cu(dca)$_2$pyz] (6). The α phase consists of two interpenetrating α-Po-related (9) networks, while the β phase contains 2D sheets. Both phases show only weak antiferromagnetic coupling. During the course of the present work, Miller and co-workers reported on the compound α-[Mn(dca)$_2$pyz], which is topologically (but not crystallographically) identical to the α-Cu phase. They presented data to show that it behaves as an ordered antiferromagnet at temperatures below 2.7 K (7). We now report the results of our extended investigation into the synthesis, structures, and magnetic properties of the compounds α-[*M*(dca)$_2$pyz] (*M* = Mn, Fe, Co, Ni, Zn) and β-[*M*(dca)$_2$pyz] (*M* = Co, Ni, Zn).

EXPERIMENTAL

Synthesis of α-Metal(II) Bis(dicyanamido) Pyrazine Complexes

α-[*Mn*(*dca*)$_2$*pyz*] **1**. A warm aqueous solution (5 ml) of Mn(ClO$_4$)$_2$.6H$_2$O (350 mg, 0.97 mmol) was added to a warm aqueous solution (5 ml) of Na(dca) (150 mg, 1.68 mmol) and pyrazine (77 mg, 0.96 mmol). Pale yellow needles formed on cooling. The yield was 106 mg, 47%. Infrared spectrum (nujol, cm^{-1}): 3604vw, 3073vw, 2408vw, 2324m, 2310m, 2247m, 2236m, 2180s,sh, 2171s, 1417m, 1388m, 1160w, 1126w, 1084w, 1054m, 922vw, 807m. Elemental analysis: Calculated for MnC$_8$H$_4$N$_8$: C, 36.0; H, 1.5; N, 42.0. Found: C, 36.0; H, 1.1; N, 41.8.

[1] To whom correspondence should be addressed.

0022-4596/01 $35.00

α-[*Fe*(*dca*)$_2$*pyz*] **2**. A warm aqueous solution (5 ml) of $Fe(ClO_4)_2.6H_2O$ (230 mg, 0.63 mmol) was added to a warm aqueous solution (7 ml) of Na(dca) (100 mg, 1.12 mmol) and pyrazine (46 mg, 1.12 mmol). Fine orange brown needles formed on cooling. The yield was 90 mg, 60%. Infrared spectrum (nujol, cm^{-1}): 3631vw, 3085vw, 2408vw, 2327m, 2248m, 2186s, 1418m, 1397m, 1162w, 1125w, 1085w, 1055m, 920vw, 807m. Elemental analysis: Calculated for $FeC_8H_4N_8$: C, 35.9; H, 1.5; N, 41.8. Found: C, 35.9; H, 1.3; N, 41.7.

α-[*Co*(*dca*)$_2$*pyz*] **3**. A hot aqueous solution (7 ml) of $Co(NO_3)_2.6H_2O$ (190 mg, 0.65 mmol) was added to a hot aqueous solution (10 ml) of Na(dca) (100 mg, 1.12 mmol) and pyrazine (47 mg, 0.59 mmol). Fine pink needles formed on cooling. The yield was 40 mg, 26%. Infrared spectrum (nujol, cm^{-1}): 3639vw, 3087vw, 2405vw, 2328m, 2252m, 2190s, 1419m, 1397m, 1164w, 1126m, 1086w, 1058m, 920vw, 816m, 809m. Elemental analysis: Calculated for $CoC_8H_4N_8$: C, 35.4; H, 1.5; N, 41.3. Found: C, 35.2; H, 0.8; N, 41.3.

α-[*Ni*(*dca*)$_2$*pyz*] **4**. A hot aqueous solution (10 ml) of Na(dca) (100 mg, 1.12 mmol) and pyrazine (48 mg, 0.60 mmol) was added to a hot aqueous solution (5 ml) of $Ni(NO_3)_2.6H_2O$ (163 mg, 0.56 mmol). A blue microcrystalline product formed soon after addition. The yield was 49 mg, 32%. Infrared spectrum (nujol, cm^{-1}): 3641vw, 2329m, 2258m, 2198s, 1419m, 1396m, 1166w, 1125m, 1088w, 1062m, 917vw, 820m, 811m. Elemental analysis: Calculated for $NiC_8H_4N_8$: C, 35.5; H, 1.5; N, 41.4. Found: C, 35.2; H, 1.3; N, 43.2.

α-[*Zn*(*dca*)$_2$*pyz*] **5**. A hot aqueous solution (5 ml) of $Zn(NO_3)_2.6H_2O$ (176 mg, 0.59 mmol) was added to a hot aqueous solution (10 ml) of Na(dca) (100 mg, 1.12 mmol) and pyrazine (48 mg, 0.60 mmol). Colorless/white needles formed on cooling. The yield was 32 mg, 21%. Infrared spectrum (nujol, cm^{-1}): 3631vw, 3610vw, 3453vw, 2329m, 2311m, 2254m, 2240m, 2194s, 2181sh, 1418m, 1394m, 1382m, 1316vw, 1166w, 1126w, 1088w, 1059m, 919vw, 813m. Elemental analysis: Calculated for $ZnC_8H_4N_8$: C, 34.6; H, 1.5; N, 40.4. Found: C, 34.6; H, 1.4; N, 40.5.

Crystals suitable for X-ray crystallography for compounds **1–3** were grown by a slow diffusion method. Aqueous solutions of the metal salt were layered with water, methanol, and finally with a methanol solution of Na(dca) and pyrazine. The overall ratio of *M*:dca:pyrazine was 1:2:1.

1.2. Synthesis of β-Metal(II) Bis(dicyanamido) Pyrazine Complexes

β-[*Co*(*dca*)$_2$*pyz*] **6**. A solution of bis(triphenylphoshoranylidene)ammonium dicyanamide [PPN][dca] (340 mg, 0.562 mmol) and pyrazine (24 mg, 0.30 mmol) in acetone (13 ml) was added to a solution of $Co(NO_3)_2.6H_2O$ (95 mg, 0.33 mmol) in acetone (8 ml). A pale pink powder formed immediately. The yield was 50 mg, 66%. Infrared spectrum (nujol, cm^{-1}): 3569vw, 3099vw, 2296s, 2248m, 2189s, 1415m, 1334s, 1165w, 1126w, 1088w, 1060m, 948vw, 808m. Elemental analysis: Calculated for $CoC_8H_4N_8$: C, 35.4; H, 1.5; N, 41.3. Found: C, 35.1; H, 1.6; N, 40.2.

β-[*Ni*(*dca*)$_2$*pyz*] **7**. A solution of [PPN][dca] (340 mg, 0.562 mmol) and pyrazine (24 mg, 0.30 mmol) in acetone (13 ml) was added to a solution of $Ni(NO_3)_2.6H_2O$ (85 mg, 0.29 mmol) in acetone (8 ml). A pale blue powder formed immediately. The yield was 74 mg, 97%. Infrared spectrum (nujol, cm^{-1}): 3571vw, 3105vw, 2295s, 2254m, 2194s, 1415m, 1330s, 1167w, 1126m, 1090w, 1063m, 950vw, 810m. Elemental analysis: Calculated for $NiC_8H_4N_8$: C, 35.5; H, 1.5; N, 41.4. Found: C, 33.8; H, 1.7; N, 38.8.

β-[*Zn*(*dca*)$_2$*pyz*] **8**. A few small prismatic crystals, suitable for single-crystal X-ray analysis, were found to exist as a trace impurity amongst fine needles of α-[Zn(dca)$_2$pyz].

1.3. X-Ray Structural Analyses

Single-crystal structural analyses for compounds **1**, **2**, **3**, and **8** were performed with a Nonius KappaCCD diffractometer using graphite-monochromated Mo*Kα* radiation ($\lambda = 0.71073$ Å), ϕ rotations with 1° frames, and a detector-to-crystal distance of 29 mm. Where data were collected at different temperatures (i.e., **1** and **2**), the same crystal was used for each study except for **1** at 173 K where another crystal was used. The data were collected, processed, and corrected for Lorentz and polarization effects using COLLECT and DENZO software (10). All crystals were face-indexed and numerical absorption corrections applied using the XPREP program (11). Structures were solved and refined using Fourier techniques within teXsan software (12), while the final full-matrix least-squares refinements on F^2 were performed with SHELXL-97 (13). All nonhydrogen atoms were refined anisotropically. Hydrogen atoms were assigned to calculated positions with isotropic thermal parameters fixed at 1.2 times that of the respective adjoining carbon atoms, except for **8** where the hydrogen atom was freely refined (isotropically). The correct space group for each data set for the α-compounds was assigned by analysis of the *hk*0 reflections, which, in this case, distinguished between the monoclinic $P2_1/n$ and orthorhombic *Pnma* systems. The lower temperature solutions were refined in monoclinic $P2_1/n$ as pseudo-merohedral twins using the twin law {100, 0–10, 00–1}, with the twin component parameters (BASF) refining to between 0.4 and 0.5. The respective higher temperature solutions were refined in orthorhombic *Pnma*, with the dicyanamide carbon and amide nitrogen atoms refined at half-occupancy since they are disordered about a mirror plane. In the case of compound

2 at 298 K, the pyrazine ligand is also disordered over two positions, hence the carbon/hydrogen atoms were accordingly also refined/included at half-occupancy. Further crystallographic details for **1–3** and **8**, at various temperatures, can be found in Table 1.

Powder X-ray diffraction data were collected at room temperature on bulk samples of **1–7** with a Scintag automated powder diffractometer using Cu$K\alpha$ radiation ($\lambda = 1.54059$ Å). The programs CrystalDiffract (14) and UnitCell (15) were used to refine unit cells for **4–7**, as shown in Table 2, using appropriate known cells as starting points, while similar analysis for **1–3** was used to confirm that single crystals were representative of bulk samples. The powder X-ray diffractogram for **5** revealed the presence of a small amount of impurities, however the majority of the peaks were used to index the cell of α-[Zn(dca)$_2$pyz] given in Table 2.

Crystallographic data for **1–3** and **8** reported in this paper have been deposited with the Cambridge Crystallographic Data Centre. The reference numbers are CCDC 153145–153148 (**1** at 123, 173, 223, and 295 K, respectively), CCDC 153149–153151 (**2** at 173, 223, and 298 K, respectively), CCDC 153152 (**3**), and CCDC 153153 (**8**). Copies of the data can be obtained free of charge on application to CCDC, 12 Union Road, Cambridge CB2 1EZ, UK (fax: (+44) 1223 336–033; e-mail: deposit@ccdc.cam.ac.uk).

1.4. Mössbauer and Magnetic Measurements

Mössbauer spectra were kindly measured by Associate Professor J.D. Cashion, Physics Department, Monash University. Isomer shifts are calibrated relative to α-iron.

Magnetic susceptibility measurements were made in the range 2–300 K using a Quantum Design MPMS 5 SQUID magnetometer with an applied field of 1 T. The powdered samples were contained in a gelatin capsule that was held in the center of a drinking straw and fixed to the end of the sample rod. Measurements of the magnetization, with field cooling (FCM) and zero-field cooling (ZFCM), in an applied field of 5 Oe were carried out to test for the presence of long-range magnetic order. High-field magnetization isotherms were measured in fields of 0–5 T.

RESULTS AND DISCUSSION

Synthesis and Characterization

Reaction of sodium dicyanamide, metal(II) nitrate or perchlorate, and pyrazine in water in a 2:1:1 mole ratio leads to formation of α-[M(dca)$_2$pyz]. These compounds can be obtained as microcrystalline powders in high yield using relatively concentrated solutions, or as fine needles in lower yield using a more dilute method. Larger crystals for X-ray studies can be obtained by slowly diffusing methanolic solutions of the ligands into aqueous solutions of the metal salts. No transformations to the β isomers were observed as previously reported for [Cu(dca)$_2$pyz] (6) where, upon standing for several days in the aqueous reaction mixture, green α-[Cu(dca)$_2$pyz] completely transformed into blue β-[Cu(dca)$_2$pyz]. The preparation of α-[Zn(dca)$_2$pyz] did, however, contain traces of β-[Zn(dca)$_2$pyz].

The β isomers for cobalt and nickel were formed by reaction of bis(triphenylphoshoranylidene)ammonium dicyanamide [PPN][dca], metal(II) nitrate, and pyrazine in acetone in a 2:1:1 mole ratio. The compounds were obtained in moderate yield as fine powders and, although the data were weak, powder X-ray diffraction confirmed these to be isomorphous with β-[Zn(dca)$_2$pyz].

The compounds give well resolved IR and Raman spectra, with characteristic IR bands from the dca moiety being listed in Table 3. The main difference between the α and β isomers can be seen in the ν_s(C–N) and ν_{as}(C–N) vibrations. For the α isomers they range from 917 to 922 cm^{-1} and 1379 to 1397 cm^{-1}, respectively, while for the β isomers they are 939 to 950 cm^{-1} and 1330 to 1340 cm^{-1}. These differences between the isomers also carry over to combination bands while the nitrile bands are similar for both.

X-Ray Crystallography

The data for the α compounds were initially collected at low temperature (123 or 173 K). Analysis of the data indicated that these systems were monoclinic $P2_1/n$ and not orthorhombic as the cell dimensions suggested. The solutions obtained in $P2_1/n$ showed apparent disorder of the dicyanamide ligands, but attempts to model this disorder were not satisfactory with varying thermal parameters and high R values ($R_1 > 0.10$). The solutions were then refined as pseudo-merohedral twins using the twin law {100, 0–10, 00–1}, which resulted in single well-refined atom positions (i.e., no disorder) with excellent thermal parameters. The R values were also low, indicating the correct interpretation of the data. The twin law {100, 0–10, 00–1} means that the structure is related to its twin component by inversion of both the b and c axes. This can occur in monoclinic systems when β is close to 90° (16), resulting in overlapping data. A preliminary solution for **1** appeared recently (7). Data were collected at 198 K and correctly interpreted as $P2_1/n$, but as the authors failed to recognize the twinning, their disordered solution was incorrect and their refinement inferior to that presented here.

We also collected data at higher temperatures for **1** and **2** and found that the dca ligands are truly disordered about the *ab* plane and in the case of **2** at 298 K the pyrazine ligand is also disordered over two positions related by an approximate 90° rotation (Fig. 1). The higher temperature data were consistent with the orthorhombic *Pnma* space group and refined well as a disordered model. The disorder is

TABLE 1
Crystallographic Information

	1	1	1	1	2	2	2	3	8
Temperature (K)	123(2)	173(2)	223(2)	295(2)	173(2)	223(2)	298(2)	123(2)	123(2)
Formula	$MnC_8H_4N_8$	$MnC_8H_4N_8$	$MnC_8H_4N_8$	$MnC_8H_4N_8$	$FeC_8H_4N_8$	$FeC_8H_4N_8$	$FeC_8H_4N_8$	$CoC_8H_4N_8$	$ZnC_8H_4N_8$
M	267.13	267.13	267.13	267.13	268.04	268.04	268.04	271.12	277.56
Crystal system	Monoclinic	Monoclinic	Orthorhombic	Orthorhombic	Monoclinic	Monoclinic	Orthorhombic	Monoclinic	Orthorhombic
Space group	$P2_1/n$	$P2_1/n$	*Pnma*	*Pnma*	$P2_1/n$	$P2_1/n$	*Pnma*	$P2_1/n$	*Cmmm*
a (Å)	7.3339(4)	7.3378(3)	16.8975(7)	16.9607(8)	7.1848(4)	7.2009(4)	17.1648(9)	7.0965(4)	7.1189(2)
b (Å)	16.7917(11)	16.8403(9)	7.3465(2)	7.3660(2)	16.6920(13)	16.7422(13)	7.2124(2)	16.6139(9)	9.6994(4)
c (Å)	8.7861(5)	8.7887(5)	8.7922(3)	8.8011(4)	8.6952(6)	8.7064(6)	8.7168(4)	8.6342(5)	7.3988(3)
α (°)	90	90	90	90	90	90	90	90	90
β (°)	90.040(4)	90.006(4)	90	90	90.041(5)	90.117(4)	90	90.047(3)	90
γ (°)	90	90	90	90	90	90	90	90	90
U (Å^3)	1082.00(11)	1086.03(10)	1091.44(7)	1099.54(8)	1042.80(12)	1049.63(12)	1079.13(8)	1017.98(10)	510.88(3)
Z	4	4	4	4	4	4	4	4	2
D_{calc} (Mgm^{-3})	1.640	1.634	1.626	1.614	1.707	1.696	1.650	1.769	1.804
μ(Mo$K\alpha$) (mm^{-1})	1.209	1.205	1.199	1.190	1.435	1.426	1.387	1.674	2.392
F(000)	532	532	532	532	536	536	536	540	276
Crystal size									
max (mm)	0.28	0.60	0.28	0.28	0.21	0.21	0.21	0.18	0.17
mid (mm)	0.16	0.18	0.16	0.16	0.13	0.13	0.13	0.06	0.08
min (mm)	0.013	0.04	0.013	0.013	0.04	0.04	0.04	0.025	0.06
θ range (°)	1.2–30.0	1.2–25.0	3.3–32.0	2.4–30.0	1.2–30.1	1.2–30.1	2.4–30.0	1.2–30.0	2.8–30.0
Index range									
h	−9, 10	−7, 7	−20, 23	−16, 23	−8, 9	−8, 8	−18, 24	−9, 9	−9, 7
k	−23, 17	−20, 19	−8, 10	−9, 9	−16, 23	−23, 18	−9, 8	−23, 23	−13, 13
l	−12, 12	−10, 10	−12, 12	−10, 12	−12, 12	−12, 12	−12, 11	−12, 12	−10, 10
T_{min}/T_{max}	0.811/0.984	0.804/0.953	0.834/0.984	0.840/0.985	0.819/0.944	0.820/0.944	0.824/0.946	0.857/0.958	0.786/0.882
Data collected	7883	7066	12043	8118	7542	7557	7458	13963	4079
Unique data (R_{int})	2888 (0.0465)	1805 (0.0258)	1785 (0.042)	1674 (0.089)	2750 (0.0502)	2898 (0.0554)	1630 (0.0596)	2924 (0.064)	453 (0.026)
Observed data [$I > 2\sigma(I)$]	2390	1718	1428	1085	2106	2149	1185	2232	448
Parameters	155	155	112	112	155	155	130	155	33
Twin component (BASF)	0.486	0.507			0.478	0.429		0.432	
Final R_1, wR_2 [$I > 2\sigma(I)$]	0.0429, 0.0621	0.0239, 0.0548	0.0493, 0.0681	0.0515, 0.0635	0.0360, 0.0605	0.0441, 0.0610	0.0587, 0.1399	0.0455, 0.0678	0.0200, 0.0472
R_1, wR_2 (all data)	0.0625, 0.0655	0.0262, 0.0556	0.0756, 0.0735	0.1055, 0.0738	0.0625, 0.0665	0.0771, 0.0668	0.0928, 0.1495	0.0760, 0.0749	0.0204, 0.0474
Goodness of fit, S	1.060	1.068	1.111	1.050	1.012	1.022	1.177	1.030	1.108
$\Delta\rho_{min}$, $\Delta\rho_{max}$ (e Å^{-3})	−0.398/0.391	−0.249/0.308	−0.511/0.455	−0.365/0.374	−0.476/0.418	−0.482/0.469	−1.499/0.626	−0.548/0.475	−0.517/0.493

TABLE 2
X-Ray Powder Diffraction Data

	4	5	6	7
Temperature (K)	295(2)	295(2)	295(2)	295(2)
Formula	$NiC_8H_4N_8$	$ZnC_8H_4N_8$	$NiC_8H_4N_8$	$CoC_8H_4N_8$
M	270.88	277.56	270.88	271.12
Crystal system	Orthorhombic	Orthorhombic	Orthorhombic	Orthorhombic
a (Å)	17.018(9)	16.773(8)	7.015(7)	7.128(7)
b (Å)	7.015(6)	7.072(5)	9.766(8)	9.758(5)
c (Å)	8.619(4)	8.675(5)	7.343(10)	7.317(8)
U (Å^3)	1028.8(9)	1028.9(8)	503.0(8)	508.9(7)

dynamic since the atoms move into ordered positions at lower temperature. When this occurs domains within each crystal order into one of two possible orientations that are related by the twin law. The phase change from orthorhombic to monoclinic therefore induces twinning of the crystals. The crystal of **2** was initially solved at 173 K with a twin component of 0.478. Following this, it was solved at 298 K, then cooled again, and solved at 223 K where it was again monoclinic but with a twin component of 0.429. This difference in twin components indicates that each domain within the crystal does not necessarily assume the same orientation each time the crystal is cooled below the phase change. The temperatures of the phase change have not been determined, but are assumed to be around 220 K, since at 223 K **1** is orthorhombic, while **2** is monoclinic. These would also then be similar to the temperature of the phase transition that occurs in β-Zn(dca)$_2$ where a similarly disordered dca ligand becomes ordered between 210 and 220 K (3a).

Structures

The atom numbering schemes for all structures are shown in Fig. 1. The structures of the α-compounds consist of two identical interpenetrating α-Po related networks (Fig. 2). The metal atoms are octahedral. Each metal is coordinated to four equatorial dca ligands, bonding via the nitrile nitrogens, and two axial pyrazine ligands. All the ligands act as two-connecting bridges. Each metal atom is connected to four others by four different dca ligands to form 2D (4,4) sheets of M(dca)$_2$. These sheets are then cross-linked by the pyrazine bridges to give an overall 3D cubic-like network. The large space within a single network allows the interpenetration of the second net. Single crystals large enough for X-ray study for the α isomers of Ni and Zn could not be obtained; however they were shown by powder diffraction to have cell parameters similar to those of Mn and Fe (Table 2).

β-[Zn(dca)$_2$pyz] contains a 2D sheet structure. Again, the metal atoms are octahedral, coordinated to four equatorial, bridging dca ligands and two axial pyrazine bridges. This time, however, each Zn atom is connected to only two others by the four different dca ligands, to give 1D chains of Zn(dca)$_2$. These chains are linked together by the two pyrazine ligands, giving the 2D sheet topology (Fig. 3). These sheets pack together parallel to each other such that the dca ligands of adjacent sheets interdigitate (Fig. 3). Again, the dca ligands coordinate only via the nitrile nitrogens. The structures of the β isomers of Co and Ni were shown to be isostructural by powder diffraction (Table 2). Although they have topologically identical structures to those reported here, the α and β phases of [Cu(dca)$_2$pyz] are not crystallographically isomorphous with any of the phases described here, most likely due to the effects of the Jahn–Teller distortion of the Cu (6).

Selected bond lengths, angles, and metal-to-metal distances for all structures are given in Table 4. For all compounds the M–N_{pyz} distances are slightly longer than the M–N_{dca} distances, with this being more pronounced in **1**, where at 123 K the M–N_{pyz} distances are 2.272(2) Å and 2.283(2) Å, compared to M–N_{dca} distances ranging from 2.168(2) Å to 2.220(2) Å. For the α-compounds all M–N distances are unique except for the orthorhombic solutions where the two

TABLE 3
Selected IR Data (dca) (nujol, cm^{-1})

	ν_{as}(C ≡ N) + ν_{as}(C–N)	ν_s(C–N) + ν_{as}(C–N)	ν_{as}(C≡N)	ν_s(C≡N)	ν_{as}(C–N)	ν_s(C–N)
1 α-[Mn(dca)$_2$pyz]	3604	2324/2310	2247/2236	2180/2171	1388	922
2 α-[Fe(dca)$_2$pyz]	3631	2327	2248	2186	1397	920
3 α-[Co(dca)$_2$pyz]	3640	2328	2252	2190	1397	920
4 α-[Ni(dca)$_2$pyz]	3641	2329	2258	2198	1396	917
α-[Cu(dca)$_2$pyz] (6)	3627	2321	2250	2182	1379	919
5 α-[Zn(dca)$_2$pyz]	3631/3610	2329/2311	2255/2240	2194/2181	1394/1382	919
6 β-[Co(dca)$_2$pyz]	3569	2296	2248	2189	1334	948
7 β-[Ni(dca)$_2$pyz]	3571	2295	2255	2194	1330	950
β-[Cu(dca)$_2$pyz] (6)	3571	2296	2245	2183	1340	939

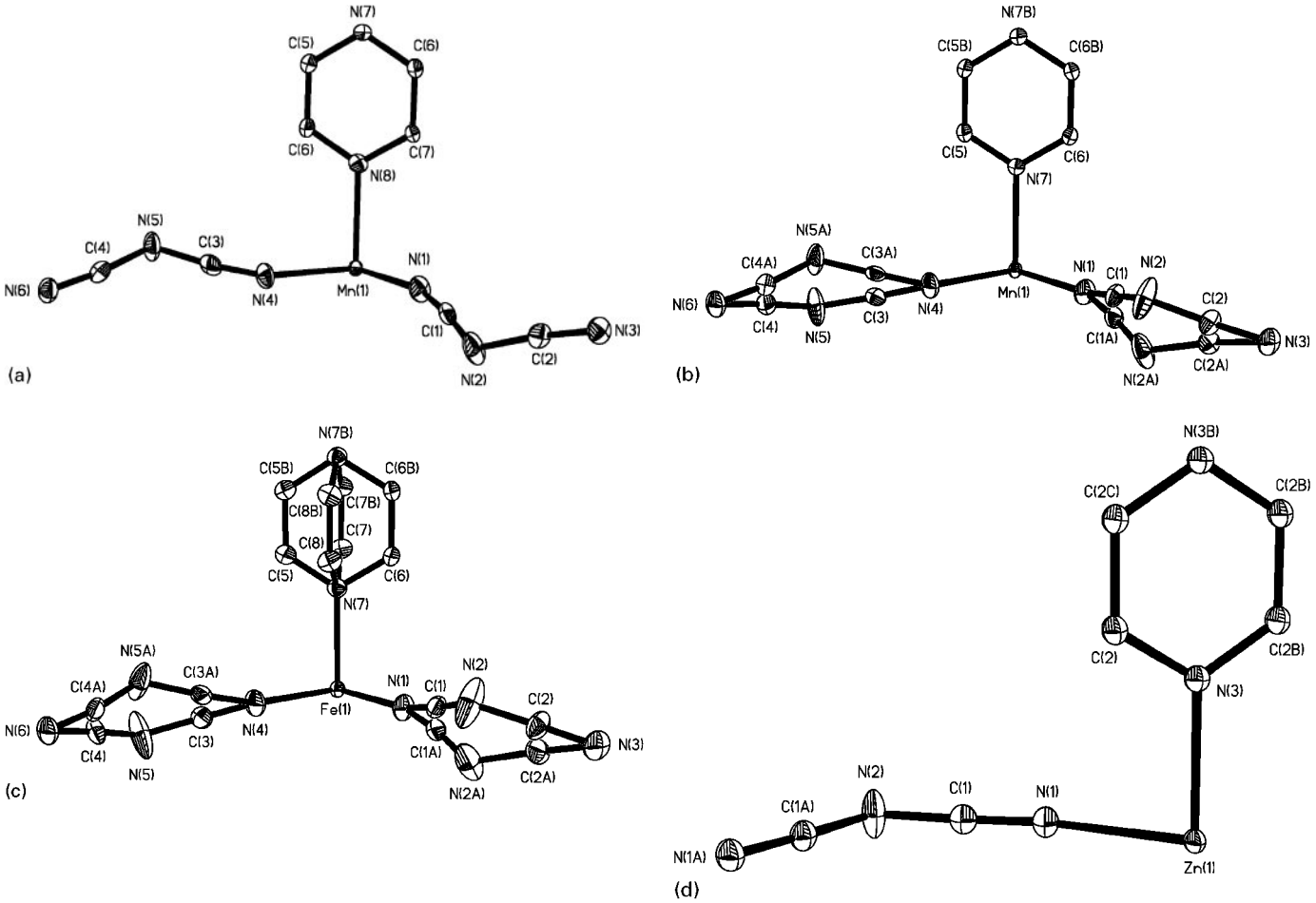

FIG. 1. Atom numbering schemes for (a) **1** at 123 K, (b) **1** at 223 K, (c) **2** at 298 K, and (d) **8**. Note the disorder in (b) and (c). Atom numbering schemes for the other structure determinations are identical to the relevant isomorphous phase shown here.

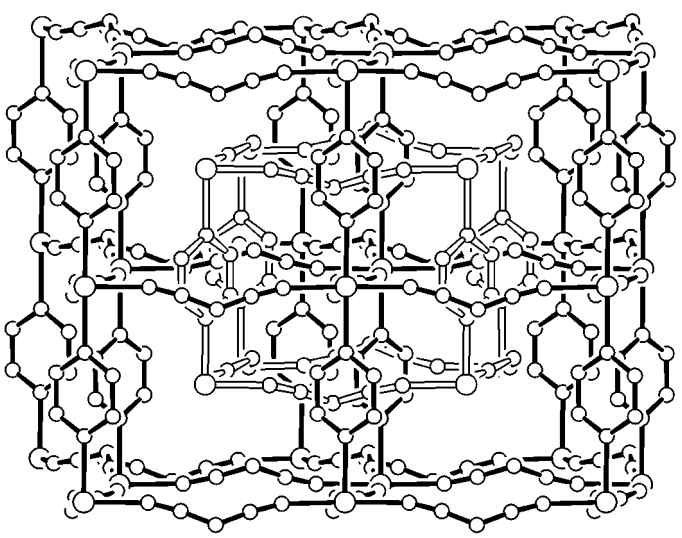

FIG. 2. Two interpenetrating α-Po-related networks in the structure of α-$[M(dca)_2pyz]$.

M–N_{pyz} distances are related by mirror plane symmetry. The structure of β-$[Zn(dca)_2pyz]$ has only one unique M–N_{pyz} distance and one unique M–N_{dca} distance due to the three perpendicular mirror planes of the *Cmmm* space group.

In structures for **1**, **2**, and **3** the C–N–M bond angles for the dca ligands range from 144° to 169°, except for **2** at 298 K where the lowest angle is 154°. This change would appear to be associated with the disorder of the pyrazine ligand, since C–N–M bond angles for **1** do not change significantly between 173 ($P2_1/n$) and 223 K (*Pnma*) where the only difference in the structures is the disorder of the dca ligands.

The shortest intranetwork M–M distance for all structures is via the pyrazine bridges, which correspond to the a cell dimensions for the $P2_1/n$ or *Cmmm* solutions or to the b cell dimensions for the *Pnma* solutions. These range from 7.096 Å for **3** to 7.366 Å for **1** (295 K). For each of **1**–**3**, there are two similar M–M distances via the dca ligands, the longer of which corresponds to the c cell dimension, while for **8** the c cell dimension is the only M–M distance via dca

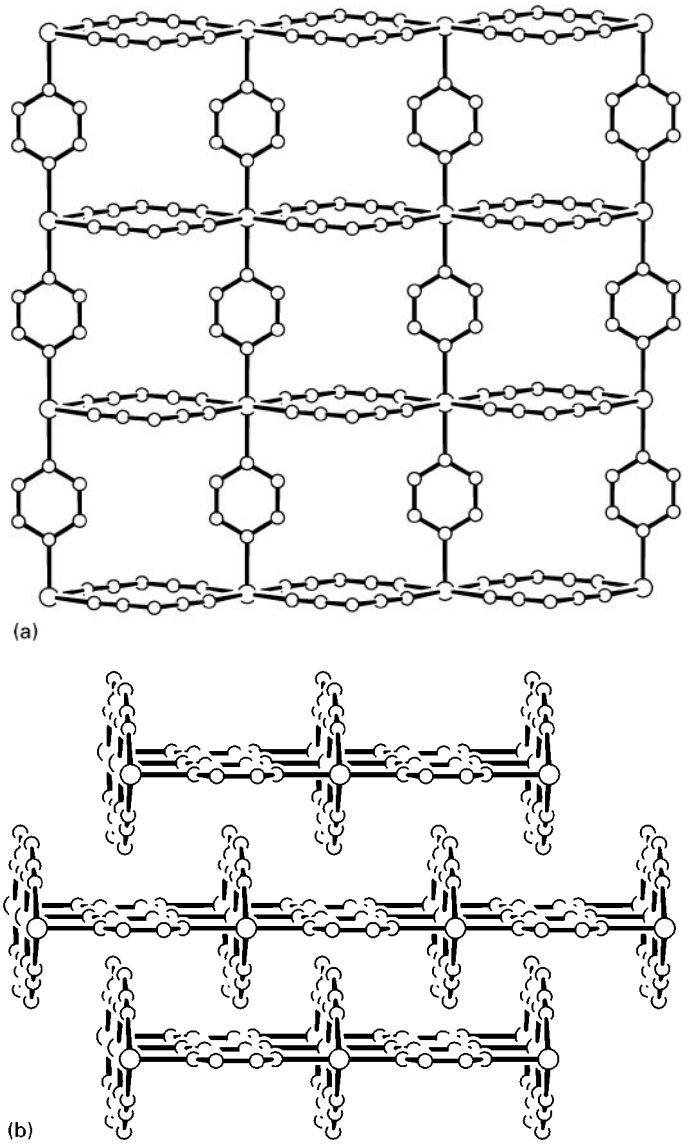

FIG. 3. (a) The sheet structure of β-[Zn(dca)$_2$pyz] **8**. (b) Interdigitation of adjacent sheets in **8**.

bridges. The shortest M–M distance, for all structures, is between networks. For monoclinic solutions of the two interpenetrating α-Po-related networks this distance ranges from 6.140 Å for **3** to 6.276 Å for **1** (173 K), while for orthorhombic solutions the range is 6.414 Å for **1** (223 K) to 6.771 Å for **2** (298 K). The disorder of the pyrazine ligands in **2** (298 K) appears to lead to a significant increase in the shortest M–M distance relative to the other solutions. In the case of **8** the shortest M–M distance is 6.016 Å, which is between the adjacent 2D sheet networks. This distance can be calculated from $(a^2 + b^2)^{1/2}/2$. Hence, from the powder cells for **6** and **7**, the respective shortest M–M distances are 6.01 Å and 6.04 Å.

Magnetic Properties

The divalent metal ions in these pyrazine adducts are high spin. This is confirmed by zero-field Mössbauer spectroscopy in the case of the Fe(II) α isomer for which a single symmetrical quadrupole doublet was observed, at 4.2 K, with isomer shift ($\delta = 1.20\ \mathrm{mm\,s^{-1}}$) and quadrupole splitting ($\Delta E_Q = 2.36\ \mathrm{mm\,s^{-1}}$) values typical of $S = 2$ iron(II). Such values are rather similar to those noted at 77 K for α-[Fe(dca)$_2$] ($\delta = 1.21\ \mathrm{mm\,s^{-1}}$, $\Delta E_Q = 3.17\ \mathrm{mm\,s^{-1}}$) but, since this canted-spin antiferromagnet orders magnetically below 18.8 K, its 4.2-K Mössbauer spectrum displays hyperfine splitting when measured in a zero applied field (17). Long-range order therefore seems unlikely to be occurring in **2**, at least above 4.2 K. This is borne out by the variable temperature magnetic moment data (Fig. 4), which show a temperature-independent value of μ_{Fe} of 5.6 μ_B between 300 and 50 K, then a rapid decrease to 3.5 μ_B at 2 K. There was no noteable change in μ_{Fe} at the crystallographic phase change at approx. 220 K. The corresponding χ_{Fe} versus temperature plot is Curie–Weiss-like ($\chi = C/(T - \theta)$), with $\theta = -3.0$ K and $C = 4.0\ \mathrm{cm^3\,mol^{-1}\,K}$. The high-temperature μ_{Fe} value is greater than spin-only $S = 2$ because of orbital degeneracy ($^5T_{2g}$ single-ion terms), spin–orbit coupling, and low-symmetry ligand field effects. The rapid decrease at low temperature arises through a combination of zero-field splitting and weak short-range antiferromagnetic coupling. The magnetization isotherms for **2** are shown in Fig. 5. Below 20 K, M is not linear with H, except below $H \sim 1.5$ T, but shows a gradual curvature, which, even at 2 K and $H = 5$ T, does not reach saturation but a M value of only 3.1 Nβ. Such behaviour is indicative of weak antiferromagnetic coupling combined with spin–orbit coupling effects. Measurement of magnetization in a tiny field of 5 Oe gave the same temperature dependence (2–20 K) as when measured in zero field, behaviour again indicative of a lack of long-range order.

Our magnetic data for **1** are the same as those reported by Miller and coworkers (7). In a field of 1 T the μ_{Mn} values remain essentially constant at 5.8 μ_B between 300 and 50 K, then decrease rapidly reaching 3.0 μ_B at 2 K on account of weak antiferromagnetic coupling and zero-field splitting. There is no change in μ_{Mn} at the crystallographic phase transition at approx. 220 K. The corresponding χ_{Mn} versus temperature plot shows Curie–Weiss behavior with a maximum at 2.7 K. Magnetization measurements in ZFCM and FCM ($H = 5$ Oe), down to 2 K, show no bifurcation of the type noted in the canted-spin antiferromagnet (weak ferromagnet) α-[Mn(dca)$_2$] (4b). Miller and coworkers (7) have postulated that the data are consistent with very weak antiferromagnetic coupling occurring within the 2D sheets and with 3D antiferromagnetic ordering occurring between the sheets. They deduced coupling constants of $J = -0.12\ \mathrm{cm^{-1}}$ (2D) and $J' = -0.14\ \mathrm{cm^{-1}}$

TABLE 4
Selected Bond Lengths (Å), Angles (°), and Distances (Å)

	1	1	1	1	2	2	2	3	8
Temperature (K)	123(2)	173(2)	223(2)	295(2)	173(2)	223(2)	298(2)	123(2)	123(2)
Space group	$P2_1/n$	$P2_1/n$	*Pnma*	*Pnma*	$P2_1/n$	$P2_1/n$	*Pnma*	$P2_1/n$	*Cmmm*
M(1)–N(1)	2.168(2)	2.169(2)	2.167(2)	2.171(3)	2.115(2)	2.115(2)	2.130(6)	2.079(2)	2.136(1)
M(1)–N(6)^{i}	2.199(2)	2.197(2)	2.196(3)	2.196(3)	2.133(2)	2.136(2)	2.144(5)	2.101(2)	
M(1)–N(3)^{ii}	2.214(2)	2.209(2)	2.212(2)	2.211(3)	2.143(2)	2.148(2)	2.151(6)	2.113(2)	
M(1)–N(4)	2.220(2)	2.218(2)	2.219(3)	2.216(3)	2.156(2)	2.159(2)	2.152(5)	2.128(2)	
M(1)–N(8)^{iii}	2.272(2)	2.273(2)			2.189(2)	2.203(2)		2.148(2)	
M(1)–N(7)	2.283(2)	2.282(2)	2.284(2)	2.295(2)	2.206(2)	2.212(2)	2.214(4)	2.167(2)	2.169(2)[a]
C(1)–N(1)–M(1)	164.4(3)	165.1(3)	163.3(4)	163.5(7)	164.6(3)	165.0(3)	167.0(9)	166.3(4)	163.2(1)
C(2)–N(3)–M(1)^{iv}	154.3(2)	155.4(2)	156.7(4)	157.2(6)	156.6(2)	157.3(3)	154.0(8)	155.9(3)	
C(3)–N(4)–M(1)	144.2(2)	144.5(2)	144.0(3)	145.0(4)	146.2(2)	146.5(2)	154.7(7)	147.1(2)	
C(4)–N(6)–M(1)^{v}	163.5(2)	165.8(3)	167.8(5)	168.9(12)	163.8(2)	165.7(3)	168.1(12)	163.1(3)	
M–M (dca bridge) $\{=c\}$	8.786	8.789	8.792	8.801	8.695	8.706	8.717	8.634	7.399
M–M (dca bridge)	8.650	8.662	8.676	8.694	8.574	8.590	8.659	8.531	
M–M (pyz bridge) $\{=a$ or $b\}$	7.334	7.338	7.347	7.366	7.185	7.201	7.212	7.096	7.119
M–M (shortest)	6.217	6.276	6.414	6.457	6.190	6.240	6.771	6.140	6.016

Note. Symmetry operations: $P2_1/n$: (i) $\frac{1}{2}-x, y+\frac{1}{2}, \frac{1}{2}-z$; (ii) $x, y, z+1$; (iii) $x+1, y, z$; (iv) $x, y, z-1$; (v) $\frac{1}{2}-x, y-\frac{1}{2}, \frac{1}{2}-z$. *Pnma*: (i) $\frac{1}{2}+x, y, \frac{1}{2}-z$; (ii) $x, y, z+1$; (iii) $x, \frac{1}{2}-y, z$; (iv) $x, y, z-1$; (v) $x-\frac{1}{2}, y, \frac{1}{2}-z$.

[a] Zn(1)–N(3).

(3D). We have obtained similar J values on our sample.

The μ_{Co} data for the α and β forms of $[Co(dca)_2pyz]$ are shown in Fig. 6. While the data are broadly similar, there are differences in the size of μ_{Co} at a particular temperature and in the shapes of the curves. Nevertheless, each plot is indicative of essentially uncoupled octahedral Co(II) ($^4T_{1g}$) centers, the temperature dependence in μ_{Co} arising from a combination of spin–orbit coupling and low-symmetry ligand field effects. We have observed similar data in other coordination polymers of Co(II) such as $Co(tcm)_2$ (tcm = tricyanomethanide) (18) and $Ph_4As[Co(dca)_3]$ (8b), although in these cases an unusual field dependence in μ_{Co} occurred below 20 K. A recent study of the 3D polymeric network in $[CaCo(malonate)_2(H_2O)_4]$ (19) also showed behavior similar to that shown in Fig. 6.

μ_{Ni} versus temperature data for α- and β-$[Ni(dca)_2pyz]$ are given in Fig. 7. While both plots are typical of octahedral Ni(II) $^3A_{2g}$ states (approx. 3 μ_B at 300 K), the values for the α phase are always higher than those for the β phase and show a rapid but small decrease below 20 K compared to the rapid and large decrease in the β form, the latter reaching 1.65 μ_B at 2 K. This decrease arises from zero-field splitting and weak antiferromagnetic coupling effects, the latter effect not being strong enough to give a maximum in the susceptibilities.

The magnetic data on this series of $[M(dca)_2pyz]$ species, including Cu(II) (6), show that very weak antiferromagnetic

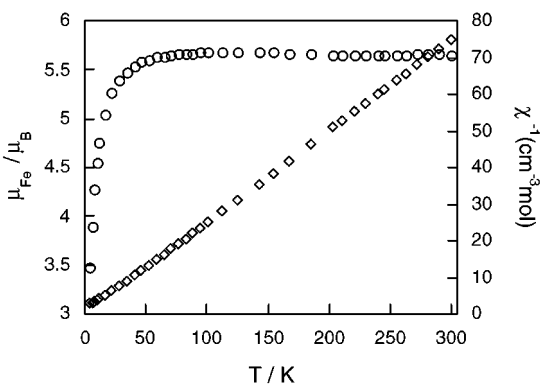

FIG. 4. Plots of magnetic moment (○) and reciprocal susceptibility (◇) versus temperature for α-$[Fe(dca)_2pyz]$ **2**, in a field of 1 T.

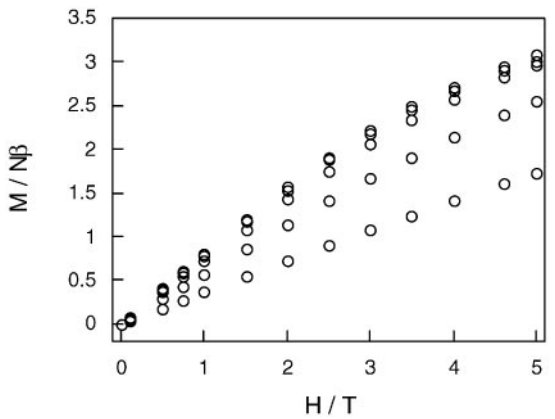

FIG. 5. Magnetization isotherms for a neat powder of **2** in fields of 0–5 T at temperatures of 2 (top), 3, 5.5, 10, and 20 K (bottom).

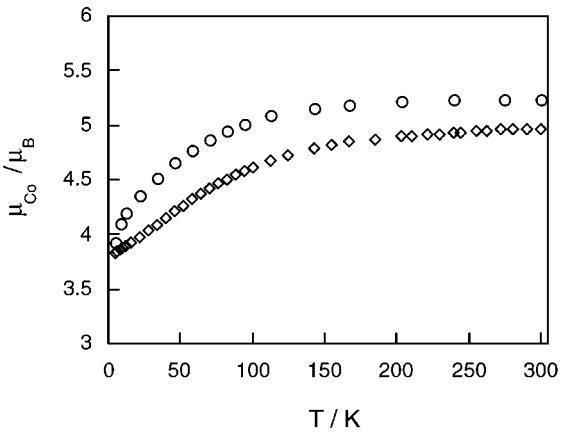

FIG. 6. Plots of μ_{Co} versus temperature for powdered samples of α-[Co(dca)$_2$pyz] (○) and β-[Co(dca)$_2$pyz] (◇) in a field of 1 T.

coupling occurs across the dicyanamide and pyrazine bridges. There are small differences in the magnetism of the interpenetrated 3D network α form and the interdigitated sheet β form (M = Co, Ni, Cu). There is no interaction between the two interpenetrating networks in the α form as far as can be ascertained, although there is some evidence for 3D antiferromagnetic order in the system with highest spin, α-[Mn(dca)$_2$pyz] (7).

None of these pyrazine-linked networks display ferromagnetic order and this is a result of the weak superexchange interactions modulated by the dca and pyz bridges combined with large M–M separations. We have noted earlier (6) the propensity for smaller anionic ligands such as CN^- and N_3^- to transmit ferromagnetic coupling. As far as the linker ligand is concerned, viz. pyrazine, 4,4-bipyridine, and pyrimidine, there appears to be a requirement for closer and more compact bridging to occur in polymeric 2D and 3D species of type [MX_2(linker)], where X = dca$^-$, NCS$^-$, N_3^-. Thus long-range magnetic order in such species is, to date, limited to compounds containing bridging pyrimidines that have a three-atom bridge. In the pair of compounds of formula [Co(NCS)$_2L$], with 2D sheet structures, that with L = pyrazine shows weak antiferromagnetic coupling of the type noted in Fig. 6, while that with L = pyrimidine shows ferromagnetic order with T_c = 8.2 K. (20). Very recently (21) a pyrimidine analogue to the present system, albeit crystallized as an ethanolate, [Fe(dca)$_2$(pyrimidine)].xEtOH, has been reported to show a magnetic phase transition at a T_c of 3.2 K. The Co(II) analogue has a T_c of 1.8 K. In these compounds 2D sheets of M(dca)$_2$ are linked by μ-1,3-pyrimidine bridges to form a 3D network. Once again, the pyrimidine bridge yields stronger coupling than does the pyrazine bridge and of a ferromagnetic sign. Long-range order has also been claimed recently in the 2D layered compound [Fe(μ-1,1-N$_3$)$_2$(pyz)], in which, as anticipated earlier (6), the azide bridge leads to ferromagnetically coupled chains, while the pyrazine linkers give antiferromagnetically coupled layers (22).

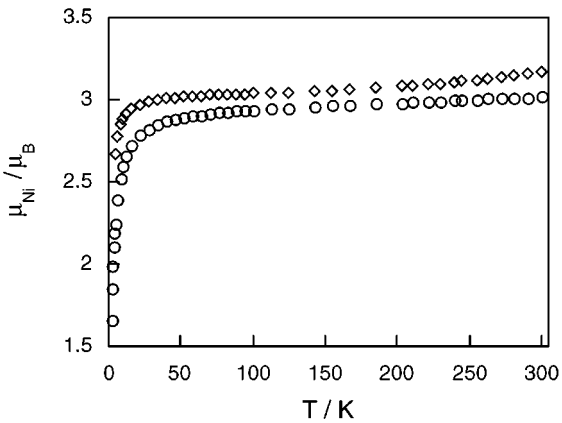

FIG. 7. Plots of μ_{Ni} versus temperature for α-[Ni(dca)$_2$pyz] (◇) and β-[Ni(dca)$_2$pyz] (○) in a field of 1 T. The corresponding χ_{Ni}^{-1} plots are Curie–Weiss like with a gentle downward curve above 200 K for the α form. Fits to the Curie–Weiss law (2–300 K) gave the following: α form, $\theta = -4.7$ K, $C = 1.23$ cm^3 mol^{-1} K; β form, $\theta = -4.7$ K, $C = 1.15$ cm^3 mol^{-1} K.

Note added in proof. In a recent detailed study of neutron diffraction, Magnetization and specific heat on **1**, Manson and coworkers (23) confirmed the antiferromagnetic order at T_N = 2.53 K and used a quasi-ID Model to deduce $J = 0.19$ cm^{-1} ($H = -JS_1 \cdot S_2$).

ACKNOWLEDGMENTS

Financial support from the Australian Research Council (ARC) Large Grants scheme (K.S.M.) is gratefully acknowledged as is an ARC Postdoctoral Fellowship (S.R.B.). The authors thank Associate Professor J. D. Cashion for the Mössbauer effect measurements on **2**.

REFERENCES

1. (a) S. R. Batten, P. Jensen, B. Moubaraki, K. S. Murray, and R. Robson, *Chem. Commun.* 439 (1998); (b) M. Kurmoo and C. J. Kepert, *New J. Chem.* **22,** 1515 (1998); (c) M. Kurmoo and C. J. Kepert, *Mol. Cryst. Liq. Cryst.* **334,** 693 (1999); (d) J. L. Manson, C. R. Kmety, Q. Huang, J. W. Lynn, G. M. Bendele, S. Pagola, P. W. Stephens, L. M. Liable-Sands, A. L. Rheingold, A. J. Epstein, and J. S. Miller, *Chem. Mater.* **10,** 2552 (1998); (e) J. L. Manson, C. R. Kmety, A. J. Epstein, and J. S. Miller, *Inorg. Chem.* **38,** 2552 (1999); (f) C. R. Kmety, J. L. Manson, Q. Huang, J. W. Lynn, R. W. Erwin, J. S. Miller, and A. J. Epstein, *Mol. Cryst. Liq. Cryst.* **334,** 631 (1999); (g) C. R. Kmety, J. L. Manson, Q. Huang, J. W. Lynn, R. W. Erwin, J. S. Miller, and A. J. Epstein, *Phys. Rev. B* **60,** 60 (1999).
2. J. Kohout, L. Jager, M. Hvastijova, and J. Kozisek, *J. Coord. Chem.* **51,** 169 (2000).
3. (a) P. Jensen, S. R. Batten, G. D. Fallon, B. Moubaraki, K. S. Murray, and D. J. Price, *Chem. Commun.* 177 (1999); (b) J. L. Manson, D. W. Lee, A. L. Rheingold, and J. S. Miller, *Inorg. Chem.* **37,** 5966 (1998).
4. (a) K. S. Murray, S. R. Batten, B. Moubaraki, D. J. Price, and R. Robson, *Mol. Cryst. Liq. Cryst.* **335,** 313 (1999); (b) S. R. Batten, P. Jensen, C. J. Kepert, M. Kurmoo, B. Moubaraki, K. S. Murray, and D. J. Price, *J. Chem. Soc. Dalton Trans.* 2987 (1999).

5. (a) P. Jensen, S. R. Batten, B. Moubaraki, and K. S. Murray, *Chem. Commun.* 793 (2000); (b) P. Jensen, D. J. Price, S. R. Batten, B. Moubaraki, and K. S. Murray, *Chem. Eur. J.* **6,** 3186 (2000); (c) S. R. Batten, A. R. Harris, P. Jensen, K. S. Murray, and A. Ziebell, *J. Chem. Soc. Dalton Trans.* 3829 (2000); (d) J. L. Manson, A. M. Arif, and J. S. Miller, *J. Mater. Chem.* **9,** 979 (1999); (e) J. L. Manson, A. M. Arif, C. D. Incarvito, L. M. Liable-Sands, A. L. Rheingold, and J. S. Miller, *J. Solid State Chem.* **145,** 369 (1999); (f) J. L. Manson, C. D. Incarvito, A. M. Arif, A. L. Rheingold, and J. S. Miller, *Mol. Cryst. Liq. Cryst.* **334,** 605 (1999); (g) G. A. van Albada, M. E. Quiroz-Castro, I. Mutikainen, U. Turpeinen, and J. Reedijk, *Inorg. Chim. Acta* **298,** 221 (2000); (h) I. Dasna, S. Golhen, L. Ouahab, O. Pena, J. Guillevic, and M. Fettouhi, *J. Chem. Soc. Dalton Trans.* 129 (2000); (i) A. Escuer, F. A. Mautner, M. Sanz, and R. Vicente, *Inorg. Chem.* **39,** 1668 (2000); (j) S. R. Marshall, C. D. Incarvito, J. L. Manson, A. L. Rheingold, and J. S. Miller, *Inorg. Chem.* **39,** 1969 (2000); (k) A. Claramunt, A. Escuer, F. A. Mautner, N. Sanz, and R. Vicente, *J. Chem. Soc. Dalton Trans.* 2627 (2000); (l) Z.-M. Wang, J. Luo, B.-W. Sun, C.-H. Yan, S. Gao, and C.-S. Liao, *Acta Crystallogr. Sect. C* **56,** 786 (2000).
6. P. Jensen, S. R. Batten, G. D. Fallon, D. C. R. Hockless, B. Moubaraki, K. S. Murray, and R. Robson, *J. Solid State Chem.* **145,** 387 (1999).
7. J. L. Manson, C. D. Incarvito, A. L. Rheingold, and J. S. Miller, *J. Chem. Soc. Dalton Trans.* 3705 (1998).
8. (a) S. R. Batten, P. Jensen, B. Moubaraki, and K. S. Murray, *Chem. Commun.* 2331 (2000); (b) P. M. van der Werff, S. R. Batten, P. Jensen, B. Moubaraki, K. S. Murray, and E. H.-K. Tan, *Polyhedron*, in press; (c) P. M. van der Werff, S. R. Batten, P. Jensen, B. Moubaraki, and K. S. Murray, *Inorg. Chem.* **40,** 1718 (2001).
9. S. R. Batten and R. Robson, *Angew. Chem. Int. Ed.* **37,** 1460 (1998).
10. (a) R. Hooft, COLLECT Software, Nonius B V, Delft, The Netherlands, 1998; (b) Z. Otwinowski and W. Minor, *in* "Methods in Enzymology", (C. W. Carter and R. M. Sweet, Eds.). Academic Press, New York, 1996.
11. XPREP, Version 5.03. Siemens Analytical X-ray Instruments Inc., Madison, WI, 1994.
12. TeXsan: Single Crystal Structure Analysis Software, Version 1.6. Molecular Structure Corporation, The Woodlands, TX, 1993.
13. G. M. Sheldrick, SHELXL-97: Program for the Refinement of Crystal Structures, University of Göttingen, 1997.
14. D. C. Palmer, CrystalDiffract 2.1.0, CrystalMaker Software, Bicester, UK, 1999.
15. T. J. B. Holland and S. A. T. Redfern, *Mineral. Mag.* **61,** 65 (1997).
16. G. M. Sheldrick, SHELX-97 Manual, 1997.
17. D. J. Price, B.Sc. (Hons) Thesis, Monash University, 1998.
18. S. R. Batten, B. F. Hoskins, B. Moubaraki, K. S. Murray, and R. Robson, *J. Chem. Soc. Dalton Trans.* 2977 (1999).
19. I. G. de Muro, M. Insausti, L. Lezama, M. K. Urtiaga, M. I. Arriortua, and T. Rojo, *J. Chem. Soc. Dalton Trans.* 3360 (2000).
20. F. Lloret, G. De Munno, M. Julve, J. Cano, R. Ruiz, and A. Caneschi, *Angew. Chem. Int. Ed.* **37,** 135 (1998).
21. T. Kusaka, T. Ishida, D. Hashizume, F. Iwasaki, and T. Nogami, *Chem. Lett.* 1146 (2000).
22. X. Hao, Y. Wei, and S. Zhang, *Chem. Commun.* 2271 (2000).
23. J. L. Manson, Q.-Z. Huang, J. W. Lynn, H.-J. Koo, M.-H. Whangbo, R. Bateman, T. Otsuka, N. Wada, D. N. Argyriou, and J. S. Miller, *J. Am. Chem. Soc.* **123,** 162 (2001).